Effects of accretion flow on the chemical structure in the inner regions of protoplanetary disks

H. Nomura[1] * , Y. Aikawa[2], Y. Nakagawa[2] and T.J. Millar[1]

[1] Astrophysics Research Centre, School of Mathematics & Physics, Queen's University Belfast, Belfast BT7 1NN, UK
e-mail: h.nomura@qub.ac.uk
[2] Department of Earth and Planetary Sciences, Kobe University, 1-1 Rokkodai-cho, Nada, Kobe 657-8501, Japan

ABSTRACT

Aims. We have studied the dependence of the profiles of molecular abundances and line emission on the accretion flow in the hot ($\gtrsim 100$K) inner region of protoplanetary disks.
Methods. The gas-phase reactions initiated by evaporation of the ice mantle on dust grains are calculated along the accretion flow. We focus on methanol, a molecule that is formed predominantly through the evaporation of warm ice mantles, to show how the abundance profile and line emission depend on the accretion flow.
Results. Our results show that some evaporated molecules keep high abundances only when the accretion velocity is large enough, and that methanol could be useful as a diagnostic of the accretion flow by means of ALMA observations at the disk radius of $\lesssim 10$AU.

Key words. accretion disks – line: formation – molecular processes – planetary systems: protoplanetary disks

1. Introduction

Recent observations have detected a variety of molecular lines towards disks around T Tauri stars (e.g., Dutrey et al. 1997; Thi et al. 2004; Qi et al. 2008). Existing millimetre/sub-millimetre observations, which have relatively low spatial resolution, can trace only the outer region ($\gtrsim 50$AU) of the disk, while near-infrared observations with high sensitivity or high spectral resolution probe molecular lines from the planet-forming region in the disks (Lahuis et al. 2006; Gibb et al. 2007; Carr & Najita 2008). The forthcoming Atacama Large Millimeter/sub-millimeter Array (ALMA), with both high sensitivity and high spatial resolution, will make it possible to observe various molecular lines from the inner regions of the disks.

Although many models on the chemical structure of young circumstellar disks focus on the outer disk (e.g., Aikawa et al. 2002; Willacy 2007), the chemistry in the inner disks has also been studied (e.g., Markwick et al. 2002). In cold pre-stellar cores, observations suggest that many gas-phase molecules, including CO, are frozen onto dust grains (e.g., Caselli et al. 1999). Young stars and circumstellar disks are thought to be formed as a result of the collapse of such molecular cloud cores. In addition, observations of molecular lines towards disks suggest that the gas-phase molecules are frozen onto grains near the midplane of cold outer disks (e.g., Dutrey et al. 1997). However, in the inner region of the disk the dust temperature is high due to the irradiation from the central star, and the ice mantles are expected to evaporate into the gas by analogy with the molecules observed towards star-forming cores, so-called hot molecular cores and hot corinos (e.g., Millar 1993;

Ceccarelli et al. 2007), so that the chemistry in the inner disk will be characterized by this ice mantle evaporation.

Accretion flow towards a central star is important for planet formation in the disk because it is one of the possible mechanisms for the dispersal of the gas, (e.g., Hollenbach et al. 2000), while the amount of the gas in the disk influences the coagulation and settling of dust grains, which lead to planetesimal formation, and also controls gaseous planet formation as well as the orbital motion of the planets (e.g., Nakagawa et al. 1986; Kominami & Ida 2002; Papaloizou et al. 2007). Meanwhile theory has suggested that the planet forming region in the disks could be magnetorotationally stable, that is, there could be no driving source of the accretion flow (e.g., Sano et al. 2000). Therefore, it will be useful if we can identify observational evidence for the accretion flow in the inner disk in order to understand the planet formation processes.

If the gas and dust in the disks are accreting towards the central star, the ice mantle molecules, which are frozen onto dust grains in the cold outer disk, will evaporate when they are transported into the hot inner disk. The evaporated molecules will be destroyed by chemical reactions while they are migrating inwards along the accretion flow. Thus, the distributions of the molecules will trace the accretion velocity, depending on whether the timescale of the chemical reactions is shorter or longer than the accretion time. Hence, it will be possible to check the existence of accretion flow from observations of the molecular distributions in the inner disk.

In this work we study the effect of the accretion flow on the chemical structure of the inner region of young disks by modelling the chemistry, initiated by the ice evaporation, along the accretion flow. And we examine the effect on the observational properties, especially focusing on a transition

---

* Now at Department of Astronomy, Graduate School of Science, Kyoto University, Kyoto 606-8502, Japan
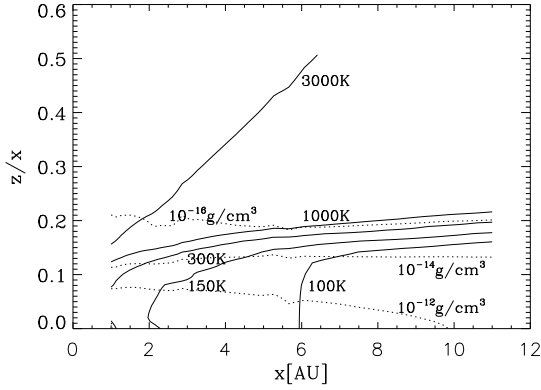
Fig. 1. Contour plots of the gas temperature (*solid lines*) and density (*dotted lines*) distributions in the z/x vs. x plane for the fiducial model with $\dot{M} = 1.0 \times 10^{-8} M_\odot$ yr^{-1}.

Table 1. Initial fractional abundances with respect to total hydrogen nuclei.

Species	Abundance	Species	Abundance
H$^+$	1.0×10^{-11}	CO	1.3×10^{-4}
He$^+$	2.5×10^{-12}	CO$_2$	3.0×10^{-6}
H$_3^+$	1.0×10^{-9}	H$_2$CO	2.0×10^{-6}
Fe$^+$	2.4×10^{-8}	CH$_3$OH	2.0×10^{-7}
He	1.0×10^{-1}	C$_2$H$_5$OH	5.0×10^{-9}
S	5.0×10^{-9}	O$_2$	1.0×10^{-6}
Si	3.6×10^{-8}	H$_2$O	2.8×10^{-4}
C$_2$H$_2$	5.0×10^{-7}	N$_2$	3.7×10^{-5}
CH$_4$	2.0×10^{-7}	NH$_3$	6.0×10^{-7}
C$_2$H$_4$	5.0×10^{-9}	H$_2$S	1.0×10^{-7}
C$_2$H$_6$	5.0×10^{-9}	OCS	5.0×10^{-8}

line of methanol, which is an abundant ice molecule in many high and low mass star forming cores (e.g., Gibb et al. 2004; Boogert et al. 2008). Methanol, which is difficult to form efficiently in the gas phase, is also known to be more abundant in the gas-phase around high and low mass young stars as well as comets (e.g., Macdonald et al. 1996; Schöier et al. 2002; Bockelee-Morvan et al. 1991) by more than orders of magnitude compared with cold dark clouds (e.g., Ohishi et al. 1992). In addition, laboratory experiments have shown that methanol can be formed in ice mantle with reasonably short timescale as a result of hydrogenation of carbon monoxide (e.g., Watanabe et al. 2006). Therefore, methanol is thought one of the most probable components of grain mantle molecules.

In the following section we introduce the physical and chemical models of the disk. We present the resulting molecular abundance profiles of the inner disk in Sect. 3 and the line emission of methanol in Sect. 4, using the models with different accretion velocities. Influence of some assumptions on the results are discussed in Sect. 5, and the results are summarized in Sect. 6.

2. Models

We model an axisymmetric disk surrounding a central star with a mass of $M_* = 1.5 M_\odot$, a radius of $R_* = 2R_\odot$, and a temperature of $T_* = 6000$K, whose luminosity ($\sim 5L_\odot$) is relatively higher than the averaged luminosity of typical T Tauri stars ($\sim 1L_\odot$) (e.g., D'Alessio et al. 2005). It is observationally known that many T Tauri stars emit strong X-ray and UV radiation. We adopt a model with black body ($T_* = 6000$K) plus thermal bremsstrahlung ($T_{\rm br} = 2.5 \times 10^4$K) emission for UV radiation ($L_{\rm FUV} = 7 \times 10^{31}$ergs s^{-1}; see Nomura & Millar 2005, hereafter NM05) and a simple thermal bremsstrahlung emission model with $T_{\rm X} = 1$keV and $L_{\rm X} = 10^{30}$ ergs s^{-1} for X-rays (Glassgold et al. 2004; Garmire et al. 2000).

The temperature and density distributions of gas and dust in the disk are obtained self-consistently as described in previous papers; see NM05 and Nomura et al. (2007) for details. Dust temperature is obtained by the iterative radiative transfer calculation (see Nomura 2002), where an initial dust temperature profile is calculated using the variable

Eddington factor method (Dullemond et al. 2002) in this work. The disk is assumed to accrete towards the central star with a constant mass accretion rate, and the α-viscous model with $\alpha = 0.01$ is adopted. The dust model which reproduces the observational extinction curve of dense clouds (see NM05) is adopted here. The resulting gas temperature and density profiles for a fiducial model with the mass accretion rate of $\dot{M} = 1.0 \times 10^{-8} M_\odot$ yr^{-1} are plotted in Figure 1.

For the chemical model we calculate the time-dependent gas-phase reactions along stream lines of steady accretion flow as

$$\frac{\partial(n_i v_{\rm acc})}{\partial l} = \sum_j k_{ij} n_j + \sum_{j,k} k_{ijk} n_j n_k, \qquad (1)$$

where n_i is the number density of the species, i, and the right hand side of the equation describes the formation and destruction of the species, i, due to cosmic-ray/photochemistry (the first term) and two-body reactions (the second term). Three-body reactions are not included, since they will not affect the result very much in the gas temperature range we treat in this work (e.g., Willacy et al. 1998). We assume that the stream lines, l, are simply described as $z = sH$, where $H = c_{s0}/\Omega_{\rm K}$ is the disk scale height, and c_{s0} the sound speed at the disk midplane, $\Omega_{\rm K}$ the Keplerian frequency. We set 60 grids for $0 \leq s \leq 3$. The equations are solved together with the continuity equation along the stream lines. The accretion velocity, $v_{\rm acc}$, is simply given by $v_{\rm acc} = \dot{M}/(2\pi\Sigma x)$, where $\dot{M}$ is the mass accretion rate, Σ the surface density of the disk, and x the distance from the central star. Turbulent mixing is not taken into account in this paper (see discussions in Sect. 5).

The chemical network consists of 208 species and is connected by 2830 reactions, in which the reaction rate coefficients are taken from the UMIST RATE06 database (http://www.udfa.net/) (Woodall et al. 2007). The X-ray ionisation is simply modelled by analogy with the cosmic-ray ionisation (see e.g., Aikawa et al. 1999 for a more detailed model). X-rays will ionise the gas and induce photoreactions, similar to cosmic-rays; we adopt the rates enhanced by $\zeta_X/\zeta_{\rm CR}$ for the reactions, where the X-ray ionisation rate, ζ_X, is calculated using the X-ray flux at each position in the disk (see Nomura et al. 2007). The H$_2$ cosmic-ray ionisation rate is set to be $\zeta_{\rm CR} = 1.3 \times 10^{-17}$ s^{-1}, and the attenuation is neglected since it is not significant except very close to the disk midplane at the disk radii of

$x \sim 1$AU in this model. As the initial condition of the calculations, the fractional abundances of the species are taken from Nomura & Millar (2004; hereafter NM04), in which the initial ice mantle composition is fixed so as to be consistent with the infrared absorption features of ices observed towards young stellar objects as well as the line emission of gas-phase molecules observed towards a hot core, G34.3+0.15 (see Table 1).

Since we particularly focus on the observational properties of a methanol line in Sect. 4, we simply start the calculations where most methanol evaporates into the gas, that is, where the timescale of the thermal evaporation of methanol, $\tau_{\rm evap}$, becomes shorter than its adsorption timescale onto dust grains, $\tau_{\rm ads}$ (see Fig. 5). The evaporation time is given by $\tau_{\rm evap} = \nu_0^{-1} \exp(E_b/kT_d)$, where ν_0 is the vibrational frequency of the adsorbed species on the grain surface. The timescale is very sensitive to the binding energy of the molecules onto the dust grains E_b, and the thermal energy of the grains, kT_d. The binding energy of methanol of $E_b/k = 4235$K is used in this work, which is experimentally measured for pure methanol ice (Sandford & Allamandola 1993). We note that the binding energy of methanol on methanol is equal to that of methanol on water ice within the error bars (W.A.Brown, private communication). The adsorption time is given by $\tau_{\rm ads} = (S\pi a^2 d_g n v_{\rm th})^{-1}$, where S is the sticking probability, $\pi a^2 d_g n$ the grain surface area per unit volume (d_g is the abundance of the dust grains relative to total hydrogen nuclei), and $v_{\rm th}$ the thermal velocity of the molecule (e.g., Tielens & Allamandola 1987). Here we use $S = 0.3$ and the averaged grain surface area per total hydrogen nuclei of $< d_g a^2 > = 2.2 \times 10^{-22}$cm^2 which is similar to that of the MRN dust model by Mathis et al. (1977) (see NM04 for details of the parameters; see also discussions in Sect. 5 for effect of dust evolution). In this model all the ice mantle molecules evaporate at the same dust temperature of $T_d \sim 85 - 100$K, depending on the local density. The influence of this simple treatment of the ice mantle evaporation is briefly discussed in Sect. 5.

3. Resulting molecular distributions

We calculate molecular abundances using the obtained density and temperature profiles. Figure 2 shows the resulting evolution of abundances of some molecules relative to total hydrogen nuclei along the stream line of $z = 1.2H$. The results for a fiducial model with the mass accretion rate of $\dot{M} = 1.0 \times 10^{-8} M_\odot$ yr^{-1} are plotted, in which the gas density and temperature range over $n \sim 3 \times 10^{11} - 1 \times 10^{13}$ cm^{-3} and $T \sim 100 - 240$K, respectively, along the flow. The gas density (n) and temperature (T) profiles as well as the distance from the central star (x) are also plotted in the figure at the bottom.

Figure 2 shows that the parent molecules which evaporate from grain surface, such as NH$_3$, H$_2$S, C$_2$H$_2$ and CH$_3$OH in this model, are relatively stable, but are eventually destroyed by reactions with ionised species or atomic hydrogen to produce daughter species, such as HCN, SO$_2$, and CH$_3$OCH$_3$, around a timescale of $\tau_{\rm chem} \sim 10^4$yr. The parent and a part of daughter species end up as CO and small hydro-carbon molecules. The timescales for the destruction of these parent molecules are nearly independent of the total density, n. This is because the number densities
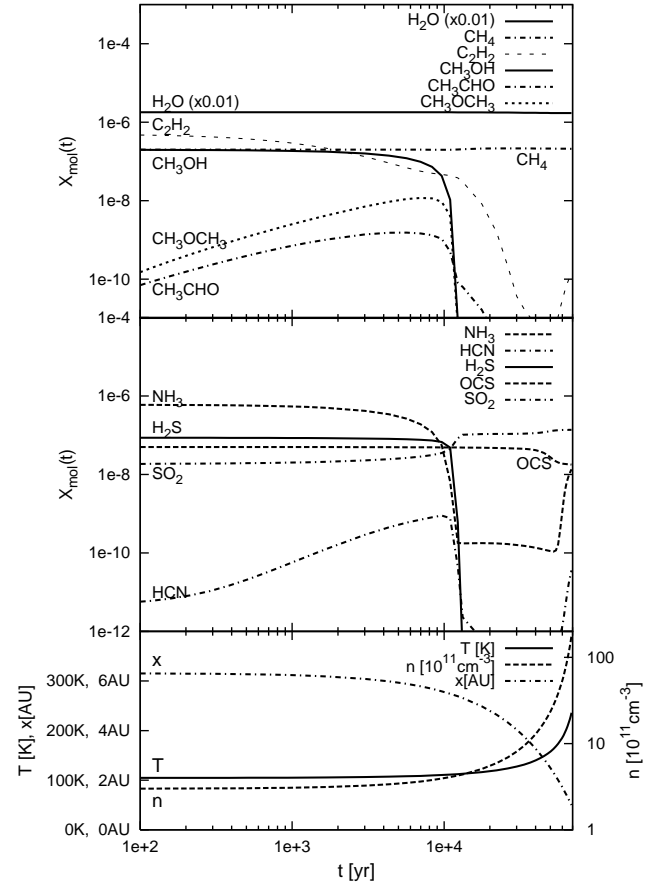

Fig. 2. Evolution of molecular abundances relative to total hydrogen nuclei along the accretion flow, $z = 1.2H$, for a model with the mass accretion rate of $\dot{M} = 1.0 \times 10^{-8} M_\odot$ yr^{-1}. The figure at the bottom shows the gas density (n) and temperature (T) profiles and the distance from the central star (x). The molecules evaporated from ice mantles are destroyed by chemical reactions around the timescale of $\sim 10^4$yr.

of ionised species and atomic hydrogen, which are formed via cosmic-ray ionisation and induced photoreactions, respectively, are not very sensitive to n. OCS is destroyed on a longer timescale than other parent molecules since its main reactant is H$_3^+$, while many of the other molecules are destroyed mainly by H$_3$O$^+$ which is more abundant than H$_3^+$. OCS does not react with H$_3$O$^+$ because its proton affinity is smaller than that of water. H$_2$O and CH$_4$ are hardly altered since they are produced efficiently in the gas-phase, especially at high temperature in the case of H$_2$O, which is formed via endothermic reactions, O $\xrightarrow{\rm H_2}$ OH $\xrightarrow{\rm H_2}$ H$_2$O. Methane is formed via the destruction of methanol and the formation processes are less temperature dependent. The abundances of NH$_3$ and HCN increase around $t \sim 10^5$yr in Figure 2 owing to endothermic reactions and high temperature in the inner disk. The detailed gas-phase chemistry induced by the evaporated molecules is similar to that occurring in hot molecular cores, which is discussed in NM04. Along $z = 1.2H$ molecules are not affected by UV and X-ray irradiation from the central star in this model (see also Sect. 4). We note that the timescales for destruction of these parent molecules by chemical reactions have

uncertainties of about an order of magnitude due to the uncertainties in the rate coefficients of the reactions (e.g., Wakalem et al. 2005).

In Figure 3, we plot the abundance profiles of some species relative to total hydrogen nuclei as a function of the disk radius along the stream line of $z = 1.2H$ for models with mass accretion rates of $\dot{M} = $ (a) 1.0×10^{-8} and (b) $5.0 \times 10^{-8} M_\odot$ yr^{-1}. In the steady accretion flow, a location of a fluid particle in the disk, x, is simply related to a time after the ice evaporation, t, as $t = \int_{x_{\text{evap}}}^{x} \{v_{\text{acc}}(x')\}^{-1} dx'$ (where x_{evap} is the evaporation radius), as shown in the bottom of Figure 2. The radial dependence of the accretion velocity is weak, and $v_{\text{acc}} \sim 40$ cm s^{-1} for the fiducial model with $\dot{M} = 1.0 \times 10^{-8} M_\odot$ yr^{-1}. In this work the accretion velocity is set to be proportional to the mass accretion rate ($v_{\text{acc}} \propto \dot{M}$) by artificially fixing the surface density of the disk to that of the fiducial model for the purpose of clear understanding of the effect of accretion flow on the chemical structure in the disk.

Figure 3 shows that the molecular abundance profiles in the inner disk change dramatically depending on the velocity of the accretion flow. When the accretion velocity is small and the accretion time, $\tau_{\text{acc}} \sim x/v_{\text{acc}}$, is longer than the timescale of the chemical reactions which destroy the evaporated molecules, τ_{chem}, the parent molecules are transported only a small distance along the accretion flow before they are destroyed by the chemical reactions. Therefore, some parent and daughter species are abundant only in the region where parent molecules are evaporated into the gas. On the other hand, if the accretion velocity is high and the accretion time is shorter than the chemical timescale, the parent molecules are transported to the central star before they are destroyed, and high abundances occur even close to the star. Some daughter species, such as HCN, become abundant gradually as the gas is transported inwards in this case. We note that the abundances of some daughter species are very sensitive to the initial fractional abundances; for example, if atomic nitrogen is abundant initially, the maximum value of the HCN abundance increases by about two orders of magnitude compared with the model we used here. Along the stream line of $z = 1.2H$, C$_2$H$_2$ is destroyed by an endothermic reaction, C$_2$H$_2$+O→CO+CH$_2$. Thus, the C$_2$H$_2$ abundance decreases, independent of the accretion rate, around $x \sim 4 - 5$AU, where the gas temperature becomes high enough for the above reaction to proceed. Along stream lines in upper layers of the disk slightly above $z = 1.2H$, where the gas density is relatively low, C$_2$H$_2$ is destroyed by reactions with molecular ions around a timescale of 10^4yr, similar to other parent molecules.

4. Methanol line emission

Using the gas density and temperature as well as the molecular abundance profiles obtained in Sect. 3, we calculate the brightness temperature of 145GHz $J_K = 3_0 - 2_0$ transition of methanol. Figure 4 shows the resulting brightness temperature of the line along a single line of sight as a function of the disk radius for models with the mass accretion rates of $\dot{M} = 1.0 \times 10^{-7}$ (solid line), 1.0×10^{-8} (dotted line), and 1.0×10^{-9} (dot-dashed line) $M_\odot$ yr^{-1}. We assume that the molecules are in the local thermal equilibrium. The assumption is reasonable since
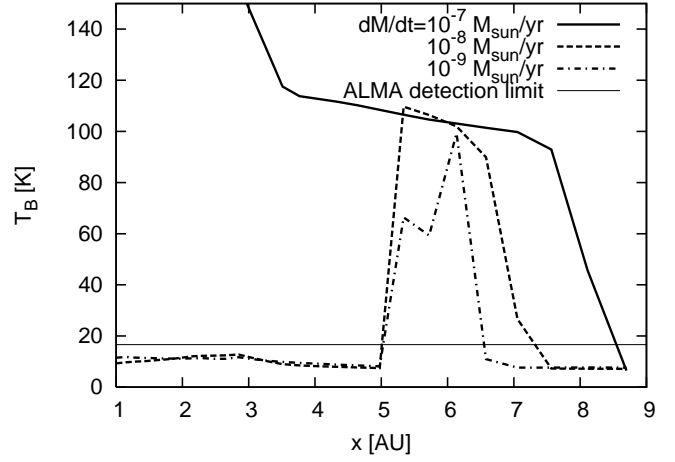

Fig. 4. Brightness temperature of the 145GHz $J_K = 3_0 - 2_0$ line of methanol calculated along a single line of sight as a function of the disk radius for models with mass accretion rates of $\dot{M} = 1.0 \times 10^{-7}$ (solid line), 1.0×10^{-8} (dotted line), and 1.0×10^{-9} (dot-dashed line) $M_\odot$ yr^{-1}. The ALMA detection limit for the beam size of ~ 14AU is also plotted with a thin solid line, showing that the line emission will be detectable in the inner disk when the accretion rate and the accretion velocity are high.

the line is emitted from regions where the density is much higher than the critical density for this transition, $n_{\text{cr}} \sim 2 \times 10^5$cm^{-3} (e.g., Pavlychenkov et al. 2007). The disk is assumed to be face-on to an observer. The molecular data is taken from Leiden Atomic and Molecular Database (http://www.strw.leidenuniv.nl/~ moldata/) (Schöier et al. 2005), and a part of the RATRAN code (http://www.sron.rug.nl/~ vdtak/ratran/ratran.html) (Hogerheijde & van der Tak 2000) is used for the line radiative transfer calculations (see NM05 for the detailed equations used in the calculations).

The figure shows that the brightness temperature of the line, T_B, is high all over the inner disk when the accretion velocity is high, while T_B becomes high just around the region where the methanol is evaporated into the gas when the accretion velocity is low, since T_B traces the abundance of methanol (see Sect. 3). Now, methanol is mainly destroyed by chemical reactions with H$_3$O$^+$, on a timescale around $\tau_{\text{chem}} \sim (kn_{\text{H}_3\text{O}^+})^{-1} \sim 10^4$yr. Here the rate coefficient is $k \sim 3 \times 10^{-9}$cm^{3}s^{-1} and the number density of H$_3$O$^+$ is $n_{\text{H}_3\text{O}^+} \sim 10^{-3}$ cm^{-3}, which is almost independent of the total number density, n, since the formation process of H$_3$O$^+$ is related to cosmic-ray ionisation. The timescale of methanol destruction is slightly affected by the abundance of NH$_3$ which helps recycle methanol by reacting with CH$_3$OH$_2^+$ (e.g., Rodgers & Charnley 2001). When the accretion rate is high, T_B is high even in slightly outer regions ($x \sim$7–9 AU) because the dust temperature is higher due to the viscous heating.

At the disk surface methanol is photodissociated due to UV and X-ray irradiation from the central star. The timescales of the dissociation are roughly given by $\tau_{\text{UV}} \sim k_{\text{UV}}^{-1} \sim 30 G_{\text{FUV}}^{-1}$ yr and $\tau_{\text{X}} \sim k_{\text{X}}^{-1} \sim 10^{-11} \zeta_{\text{X}}^{-1}$ yr, respectively, where G_{FUV} is the FUV radiation field normalized by 1.6×10^{-3} ergs s^{-1} cm^{-2} and ζ_{X} is the total hydrogen ionisation rate by X-rays. Therefore, the photodissociation dom-
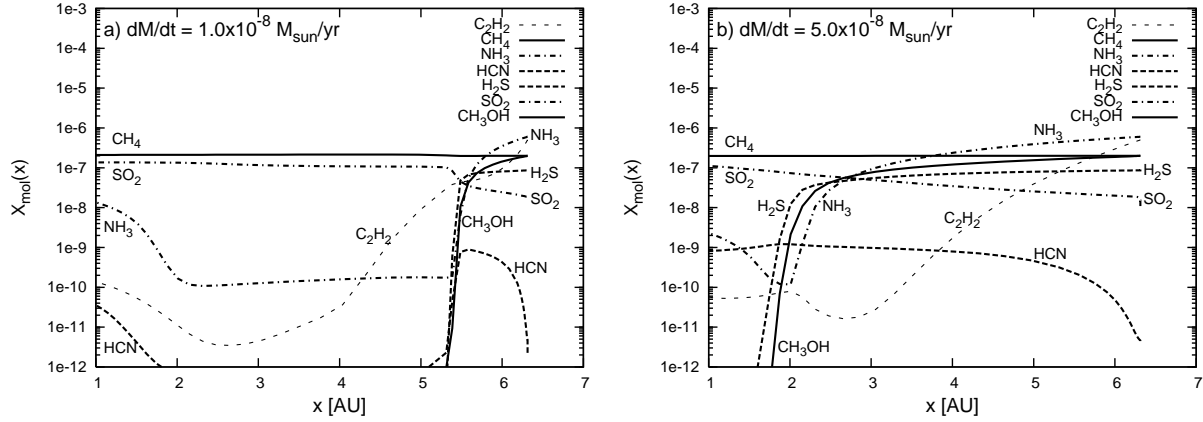
Fig. 3. Abundance profiles of some species relative to total hydrogen nuclei as a function of the disk radius along the stream line of $z = 1.2H$ for models with the mass accretion rates of $\dot{M} = $ (a) 1.0×10^{-8} and (b) $5.0 \times 10^{-8} M_\odot$ yr^{-1}. Some molecules are abundant just around the region of the ice mantle evaporation when $\dot{M}$ is low and the accretion time ($\tau_{\rm acc}$) is longer than the timescale of the chemical reactions which destroy the parent molecules, while they are abundant even close to the central star when $\dot{M}$ is high and $\tau_{\rm acc}$ is short enough.

inates the destruction of methanol where $G_{\rm FUV} \gtrsim 3 \times 10^{-3}$ or $\zeta_{\rm X} \gtrsim 10^{-15}$ s^{-1}. In Figure 5 the contour lines of $G_{\rm FUV} = 10^{-3}$ and 10^{-10} (*thin solid lines*), $\zeta_{\rm X} = 10^{-15}$ and 10^{-17} s^{-1} (*dashed lines*) are plotted in z vs x plane of the disk together with the line of $\tau_{\rm evap} = \tau_{\rm ads}$ for methanol (*thick solid line*), which corresponds to $T_d \sim 85 - 100$K, and $z = H$ (*dot-dashed line*) for the fiducial model. Figure 5 shows that the line brightness temperature at $x \gtrsim 6-7.5$AU in Figure 4 is low because the methanol can evaporate from dust grains only in the surface layer of the disk where it is dissociated quickly by strong X-ray and UV irradiation from the central star.

In Figure 4 we also plot with a thin solid line the ALMA detection limit for the methanol line, calculated using the ESO ALMA Sensitivity Calculator (http://www.eso.org/sci/facilities/alma/observing/tools /etc/index.html). The detection limit of ~ 17K is achieved when we observe for 600 sec by using 50 antennas of the 12m Array, assuming a velocity resolution of 1 km s^{-1}, and a beam size of 0.1 arcsec, which corresponds to $\sim$14AU when the disk is located at the distance of nearby star-forming regions, ~ 140 pc. The 145GHz $J_K = 3_0 - 2_0$ transition of methanol has not been detected towards DM Tau (Dutrey 2001), and other methanol line searches towards some T Tauri and Herbig Ae stars (Thi et al. 2004; Semenov et al. 2005), have also been unsuccessful. Our results suggest that when the accretion velocity at $x \leq 10$AU is high enough, ALMA can detect the methanol line, taking advantage of high spatial resolution to avoid beam dilution. When the accretion velocity is low enough, line detection will be difficult even with ALMA. Thus, the observations of methanol by ALMA could be a useful tool to diagnose the existence of accretion flows in the inner disks.

5. Discussions

In this section, we discuss some possible effects of the assumptions on our results.

First, we discuss the influences of the simple treatment of the evaporation process we have taken in this work. Although we simply assume that all the species evaporate
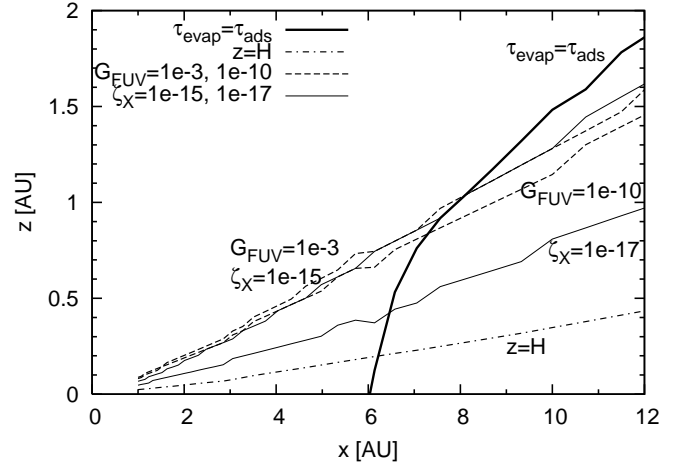

Fig. 5. Line of $\tau_{\rm evap} = \tau_{\rm ads}$ inside which the icy methanol evaporates into the gas (*thick solid line*), line of $z = H$ (*dot-dashed line*), and contour lines of $G_{\rm FUV} = 10^{-3}$ and 10^{-10} (*thin solid lines*), $\zeta_{\rm X} = 10^{-15}$ and 10^{-17} s^{-1} (*dashed lines*) for the fiducial model with $\dot{M} = 1.0 \times 10^{-8} M_\odot$ yr^{-1}. The evaporated methanol is quickly dissociated due to strong UV photons or X-rays at $x \geq 7$AU.

at the same dust temperature, the evaporation of ice mantle molecules may depend on the binding energy of each molecule and the morphology of water ice (e.g., Collings et al. 2004). Therefore, different parent molecules may evaporate at different positions (see e.g., Markwick et al. 2002), which will affect the spatial distributions of molecular abundances. In particular, CO and N_2 are likely to evaporate at temperatures much lower than 85K, particularly if they are abundant in the surface layers of the ice. However, given the chemical stability of these species, they are unlikely to affect the overall abundance of a molecule such as methanol. So, the timescales for the destruction of the parent molecules by chemical reactions, $\tau_{\rm chem}$, analysed in Sect. 3 will not be very sensitive to the treatment of the ice mantle evaporation. In addition to the evaporation process, surface chemistry involving heavy radicals on warm dust grains may

affect molecular abundances in both solid- and gas-phase (e.g., Garrod & Herbst 2006; Aikawa et al. 2008). More detailed model including the detailed evaporation process as well as surface reactions on dust grains should be constructed in future work.

Next, if we take into account the effect of turbulent mixing in the vertical direction, the methanol abundance may increase near the line, $\tau_{\mathrm{evap}} = \tau_{\mathrm{ads}}$, (see Fig. 5) when the diffusion time is shorter than the timescale of the photodissociation (e.g., Willacy et al. 2006). In the inner disk ($x \lesssim 6\mathrm{AU}$) the methanol abundance may slightly decrease via the vertical mixing because of the photodissociation at the disk surface. The turbulent mixing in the radial direction may enhance the gas-phase methanol abundance outside the evaporation radius if the timescale of the turbulent diffusion is shorter than the timescale of the chemical reactions and that of the adsorption on dust grains. A detailed mixing model which treats angular momentum transfer will be needed in order to obtain the diffusion timescale, and advance further discussion.

Finally, we note that the brightness temperature of the methanol line will reflect some conditions other than the accretion velocity: the high-T_B region becomes smaller if the central star is less luminous and the dust temperature in the disk is low. Also, T_B becomes low if the methanol abundance in the ice mantle is low. If the amount of small dust grains decreases due to the dust coagulation and settling in the disk, methanol is photodissociated by ineffectively attenuated FUV photons from the central star (e.g., Aikawa & Nomura 2006), and therefore T_B drops, although the evaporation radius moves slightly outwards owing to the decrease of the total grain surface area per unit volume, that is, the decrease of the adsorption rate (e.g., Aikawa 2007). Thus, some causes other than low accretion velocity can lead to low methanol abundance and the non-detection of the line. However, if the observed methanol abundance is high in the inner disk, then the accretion velocity must be high in the planet-forming region.

6. Conclusions

We have calculated the gas-phase chemical reactions, initiated by the ice mantle evaporation, along the accretion flow in protoplanetary disks to show that the accretion velocity affects the abundance profiles of the evaporated molecules and their daughter species in the inner disk. We have obtained the brightness temperature profile of an emission line of methanol, and suggested that this could be useful as an indicator of accretion velocity in the planet-forming regions in disks using ALMA observations.

References

Aikawa, Y. 2007, ApJ, 656, L93
Aikawa, Y. & Herbst, E. 1999, A&A, 351, 233
Aikawa, Y. & Nomura, H. 2006, ApJ, 642, 1152
Aikawa, Y., van Zadelhoff, G.J., van Dishoeck, E.F., & Herbst, E. 2002, A&A, 386, 622
Aikawa, Y., Wakelam, V., Garrod, R.T., & Herbst, E. 2008, ApJ, 674, 984
Bockelee-Morvan, D., Colom, P., Crovisier, J., Despois, D., Paubert, G. 1991, Nature, 350, 318
Boogert, A.C.A. et al. 2008, ApJ, 678, 985
Carr, J.S. & Najita, J.R. 2008, Nature, 319, 1504
Caselli, P., Walmsley, C.M., Tafalla, M., Dore, L., & Myers, P.C. 1999, ApJ, 523, L165
Ceccarelli, C., Caselli, P., Herbst, E., Tielens, A.G.G.M., & Caux, E., in Protostars and Planets V, ed. B. Reipurth, D. Jewitt, and K. Keil (Tuscon: Univ. Arizona Press), 47
Collings, M.P. et al. 2004, MNRAS, 354, 1133
D'Alessio, P., Merin, B., Calvet, N., Hartmann, L., & Montesinos, B. 2005, RMxAA, 41, 61
Dullemond, C.P., van Zadelhoff, G.J., Natta, A. 2002, A&A, 389, 464
Dutrey, A. 2001, in Science with the Atacama Large Millimeter Array, ASP Conf. Ser. 235, ed. A. Wootten (San Francisco: ASP), 215
Dutrey, A., Guilloteau, S., & Guelin, M. 1997, A&A, 317, L55
Garrod, R.T., & Herbst, E. 2006, A&A 457, 927
Garmire, G., et al. 2000, AJ, 120, 1426
Gibb, E.L., van Brunt, K.A., Brittain, S.D., & Retting, T.W. 2007, ApJ, 660, 1572
Gibb, E.L., Whittet, D.C.B., Boogert, A.C.A., & Tielens, A.G.G.M. 2004, ApJS, 151, 35
Glassgold, A.E., Najita, J., & Igea, J. 2004, ApJ, 615, 972
Hogerheijde, M. R., & van der Tak, F. F. S. 2000, A&A, 362, 697
Hollenbach, D.J., Yorke, H.W., & Johnstone, D. 2000, in Protostars and Planets IV, ed. V.G. Mannings, A.P. Boss, & S.S. Russell (Tuscon: Univ. Arizona Press), 401
Kominami, J. & Ida, S. 2002, Icarus, 157, 43
Lahuis, F. et al. 2006, ApJ, 636, L145
Macdonald, G.H., Gibb, A.G., Habing, R.J., & Millar, T.J. 1996, A&AS, 119, 333
Markwick, A. J., Ilgner, M., Millar, T. J., & Henning, T. 2002, A&A, 385, 632
Mathis, J.S., Rumpl, W. & Nordsieck, K.H. 1977, ApJ, 217, 425
Millar, T.J. 1993, in Dust and Chemistry in Astronomy, ed. T.J. Millar & D.A. Williams (Bristol: IOP Publishing), 249
Nakagawa, Y., Sekiya, M., & Hayashi, C. 1986, Icarus, 67, 375
Nomura, H. 2002, ApJ, 567, 587
Nomura, H., Aikawa, Y., Tsujimoto, M., Nakagawa, Y., & Millar, T.J. 2007, ApJ, 661, 334
Nomura, H. & Millar, T.J. 2004, A&A, 414, 409 (NM04)
Nomura, H. & Millar, T.J. 2005, A&A, 438, 923 (NM05)
Ohishi, M., Irvine, W.M., & Kaifu, N. 1992, in Astrochemistry of Cosmic Phenomena, IAU Symp. 150, ed. P.D. Singh (Dordrecht: Kluwer), 171
Papaloizou, J.C.B. et al. 2007, in Protostars and Planets V, ed. B. Reipurth, D. Jewitt, and K. Keil (Tuscon: Univ. Arizona Press), 655
Pavlychenkov, Ya. et al. 2007, ApJ, 2007, 669, 1262
Qi, C., Wilner, D., Aikawa, Y., Blake, G.A., & Hogerheijde, M.R. 2008, ApJ, 681, 1396
Rodgers, S.D., & Charnley, S.B. 2001, ApJ, 546, 324
Sandford, S.A. & Allamandola, L.J. 1993, ApJ, 417, 815
Sano, T., Miyama, S. M., Umebayashi, T., & Nakano, T. 2000, ApJ, 543, 486
Schöier, F.L., Jørgensen, J.K., van Dishoeck, E.F. & Blake, G.A. 2002, A&A, 390, 1001
Schöier, F. L., van der Tak, F.F.S., van Dishoeck, E.F., & Black, J.H. 2005, A&A, 432, 369
Semenov, D. et al. 2005, ApJ, 621, 853
Thi, W.-F., van Zadelhoff, G.-J., & van Dishoeck, E. F. 2004, A&A, 425, 955
Tielens, A.G.G.M., & Allamandola, L.J. 1987, in Interstellar Processes, ed. D.J. Hollenbach, H.A. Thoronson Jr (Reidel, Dordrecht), 397
Wakalem, V., Selsis, F., Herbst, E., & Caselli, P. 2005, A&A, 444, 883
Watanabe, N., Nagaoka, A., Hidaka, H. Shiraki, T., Chigai, T., & Kouchi, A. 2006, P&SS, 54, 1107
Willacy, K. 2007, ApJ, 660, 441
Willacy, K., Klahr, H.H., Millar, T.J., & Henning, Th. 1998, A&A, 338, 995
Willacy, K., Langer, W., Allen, M., & Bryden, G. 2006, ApJ, 644, 1202
Woodall, J., Agundez, M., Markwick-Kemper, A. J., & Millar, T. J. 2007, A&A, 466, 1197